Autophagy inhibition improves sunitinib efficacy in pancreatic neuroendocrine tumors via a lysosome-dependent mechanism

Tabea Wiedmer [1, 2], Annika Blank [1], Sophia Pantasis [1], Lea Normand [1], Ruben Bill [3], Philippe Krebs [1], Mario P. Tschan [1,2], Ilaria Marinoni [1, §], Aurel Perren [1, §]

[1] Institute of Pathology, University of Bern, Bern, Switzerland

[2] Graduate School for Cellular and Biomedical Sciences, University of Bern, Bern, Switzerland

[3] Department of Internal Medicine, Regional Hospital Emmental Burgdorf, Burgdorf, Switzerland

[§] equal contribution

Running title: Autophagy inhibition improves sunitinib efficacy in PanNET

Keywords: pancreatic neuroendocrine tumors, sunitinib, chloroquine, autophagy, lysosomal membrane permeabilization

Abbreviations: ATG: autophagy-related; BafA1: Bafilomycin A1; CQ: chloroquine; LAMP: lysosome-associated membrane protein; MAP1LC3/LC3: microtubule associated protein 1 light chain 3; LMP: lysosomal membrane permeabilization; PARP: poly ADP ribose polymerase; PDGF: platelet-derived growth factor; PanNET: pancreatic neuroendocrine tumor; VEGF: vascular endothelial growth factor.

Grant support: This work was supported by the Swiss Cancer League under Grant KFS-3360-02-2014 to Aurel Perren, Mario Tschan and Ilaria Marinoni. Ilaria Marinoni was supported by a Swiss National Science Foundation career grant (SNF-PMPDP3_164484).

Corresponding authors:

Aurel Perren
Institute of Pathology
University of Bern
Murtenstrasse 31
3008 Bern, Switzerland
Phone: +41316323223
Fax: +41316324995
Email: aurel.perren@pathology.unibe.ch

Ilaria Marinoni
Institute of Pathology
University of Bern
Murtenstrasse 31
3008 Bern, Switzerland
Phone: +41316324991
Fax: +41316324995
Email: ilaria.marinoni@pathology.unibe.ch

Abstract

Increasing the efficacy of approved systemic treatments in metastasized pancreatic neuroendocrine tumors (PanNETs) is an unmet medical need. The anti-angiogenic tyrosine kinase inhibitor sunitinib is approved for PanNET treatment. Additionally, sunitinib is a lysosomotropic drug and such drugs can induce lysosomal membrane permeabilization as well as autophagy. We investigated sunitinib-induced autophagy as a possible mechanism of PanNET therapy resistance. Sunitinib accumulated in lysosomes and induced autophagy in PanNET cell lines. Adding the autophagy inhibitor chloroquine reduced cell viability in cell lines and in primary cells isolated from PanNET patients. The same treatment combination reduced tumor burden in the Rip1Tag2 transgenic PanNET mouse model. The combination of sunitinib and chloroquine reduced recovery and induced apoptosis *in vitro*, whereas single treatments did not. Knockdown of key autophagy proteins in combination with sunitinib showed similar effect as chloroquine. Sunitinib also induced lysosomal membrane permeabilization, which further increased in the presence of chloroquine or knockdown of lysosome-associated membrane protein (LAMP2). Both combinations led to cell death. Our data indicate that chloroquine increases sunitinib efficacy in PanNET treatment via autophagy inhibition and lysosomal membrane permeabilization. We suggest that adding chloroquine to sunitinib treatment will increase efficacy of PanNET treatment and that such patients should be included in respective ongoing clinical trials.

Introduction

Pancreatic neuroendocrine tumors (PanNETs) show a neuroendocrine differentiation analogous to the cells of islets of Langerhans and represent 3% of pancreatic tumors. PanNETs have significant malignant potential and surgery is the only curative option. Despite increasing availability of therapy options, stable disease is achieved in only 30% of stage IV PanNET patients and partial remission is observed only in rare cases (1-4). Sunitinib is a multi-tyrosine kinase inhibitor targeting mainly vascular endothelial growth factor (VEGF) and platelet-derived growth factor (PDGF) receptors leading to inhibition of angiogenesis and destabilization of existing vasculature (5). Sunitinib has a dual anti-tumor effect in PanNETs targeting the vasculature as well as targeting tyrosine kinases expressed by tumor cells (6,7). Sunitinib is approved for treatment of advanced PanNETs and has been shown to prolong progression free survival (4). However, its efficacy is limited by intrinsic and acquired resistance. In Rip1Tag2 mice, a transgenic mouse model for PanNETs, mechanisms of acquired resistance towards sunitinib have been described (8-10). Sunitinib is a lysosomotropic drug, which freely diffuses the lysosomal membrane. In the lysosome, it is protonated due to the low pH, and thus accumulates due to the inability to diffuse through the membrane (11). Ellegaard et al. have shown that sunitinib inhibits acid sphingomyelinase (ASM), which influences lysosome stability (12). Sunitinib further leads to lysosomal leakage and later to mitochondrial membrane permeabilization and ultimately to cell death (12). Interestingly, cancer cell lysosomes are less stable than normal lysosomes due to transformation-associated changes in lysosome-associated membrane protein 1 (LAMP1) and LAMP2 levels as well as in sphingolipid metabolism (13-15). Lysosomotropic drugs were shown to trigger lysosomal cell death even in apoptosis- and multidrug-resistant cancer cells (15). Therefore, targeting lysosomes is considered a promising yet rather unexplored therapeutic strategy. More recently, it has been proposed that leaky lysosomes do not necessarily lead to cell death. Instead, the release of lysosomal enzymes might affect physiological functions, for example influencing invasion by degradation of focal adhesions

(16). Additionally, lysosomes undergoing lysosomal membrane permeabilization (LMP) induce autophagy and are subsequently cleared by lysophagy (17-19).

Macroautophagy, hereafter named autophagy, is mainly a cell survival mechanism activated upon cellular stress to sequester and degrade long-lived proteins and damaged organelles and to recycle nutrients (20). Autophagy can promote tumorigenesis by increasing cell survival in unfavorable environment such as hypoxia or anti-cancer treatments (21). Many anti-cancer treatments have been shown to affect autophagy *in vitro* and *in vivo*. Previously, it was found that sunitinib modulates autophagy in other cellular systems *in vitro* (22-25). However, whether the modulation of autophagy by sunitinib is due to a block or an induction of autophagy is controversial. Since autophagy can promote tumorigenesis and resistance towards anti-cancer treatments, it has been exploited as therapeutic target *in vitro*, *in vivo* and in early clinical trials. In clinical trials, the most commonly used treatments to inhibit autophagy are the anti-malaria drugs chloroquine (CQ) and hydroxychloroquine (HCQ) (26). Both are lysosomotropic compounds, which inhibit autophagy via blocking lysosomal function. The role of autophagy and response towards its inhibition depends on tumor stage. Indeed autophagy functions are initially often tumor suppressing and at later stages tumor promoting. Additionally, the role of autophagy differs between tumor types (21). The role of autophagy role in mediating sunitinib response has not been studied in PanNET yet.

In this study, we investigated whether sunitinib upregulates autophagy in PanNETs and whether this is important in mediating therapy response or resistance. We assessed whether combination with the autophagy inhibitor chloroquine enhanced the anti-tumor effect of sunitinib. Moreover, we questioned how sunitinib accumulation in lysosomes and LMP affect autophagy and treatment response.

Material & Methods

Drugs, inhibitors and antibodies

Bafilomycin A1 (B-1080) was purchased from LC Laboratories, chloroquine (C6628) from Sigma, and sunitinib (S1042) from Selleckchem.

Antibodies against ATG5 (#2630), cleaved caspase 3 (#9661 and #9664), cleaved PARP (#9541) were purchased from Cell Signaling, ATG7 (ab52472) and CD31 (ab28364) from Abcam, galectin 3 (#556904) from BD Biosciences, GAPDH (#MAB374, clone 6C5) from Millipore, LAMP2 (sc-18822) and SV40 (sc-20800) from Santa Cruz, Ki67 (#RM-9106) from Thermo Fisher Scientific and LC3B (NB600-1384) from Novus Biologicals.

Cell lines

BON1 cell line was provided by E.J. Speel, Maastricht, Netherlands in 2011. QGP1 cell line was purchased from the Japanese Health Sciences Foundation, Osaka, Japan in 2011. Short tandem repeat (STR) analysis by PCR was performed for both cell lines (QGP1 in 2011 and 2016, BON1 in 2014 and 2016). QGP1 cells were authenticated. A BON1 profile does not exist yet but the profile of these cells did not match any known profile of cancer cell lines thus excluding contamination from other lines. Additionally, expression of the specific neuroendocrine markers chromogranin A and synaptophysin were routinely tested by immunohistochemistry. BON1 cells were cultured in DMEM/F12 medium (Sigma), QGP1 cells in RPMI 1640 medium (Sigma). For both cell lines medium was supplemented with 10% FBS, 100U/ml penicillin and 0.1mg/ml streptomycin and cells were kept in a humidified incubator at 5%CO_2 and 37°C. After thawing, cells were cultured for approximately two months.

Generation of knockdown cell lines

Short-hairpin RNA (shRNA) against ATG5 (NM_004849.1-420s1c1, NM_004849.1-915s1c1, NM_004849.1-1170s1c1), ATG7 (NM_006395.1-268s1c1, NM_006395.1-491s1c1, NM_006395.1-2173s1c1) and LAMP2 (NM_002294.1-291 and NM_002294.1-561) as well as a non-targeting shRNA control (SHC002) were delivered with a lentivirus expressing vector pLKO.1 (all from Sigma, MISSION shRNA). Lentivirus production and transduction were

performed as described (27). Cells were selected with 1.5µg/ml puromycin for 3-4 days. Knockdown efficiency was validated by immunoblotting of respective proteins.

Primary cell culture

Fresh human PanNET tissue was obtained from patients who underwent surgery at the Inselspital Bern and have signed an institutional informed consent. Ethical approval was given by the cantonal authorities (Kantonale Ethikkommission Bern, Ref.-Nr. KEK-BE 105/2015). Fresh tissue was digested with collagenase IV (Worthington) and trypsin for 1h at 37°C followed by red blood lysis with ACK buffer (Gibco). Single cell suspension was plated in 96-well plates and viability was measured after 48h treatment with ATPlite assay kit (Perkin Elmer) according to manufacturer instructions. Protein extracts were collected from 96-well plates using urea lysis buffer (8M urea, 0.5% Triton X-100) and immunoblotting was performed as described. Primary tumor was from a male stage II patient (age 62, patient I) with a well-differentiated grade G2 tumor showing no hormone secretion. Liver metastasis was from a male stage IV patient (age 65, patient II), with a well-differentiated grade G3 tumor showing no hormone secretion. Despite sunitinib is currently only approved for treatment of G1 and G2 tumors, patient II was included in this study due to the well-differentiated state of the tumor. The coefficient of drug interaction (CDI) was calculated as CDI=AB/(AxB). AB is the relative viability after the combination treatment of drugs A and B, while A and B are the relative viability after single treatment with drug A and B, respectively. CDI<1 indicates a synergistic effect, CDI=1 an additive effect and CDI>1 an antagonistic effect (28).

MTT and clonogenic assay

Cells were cultured and treated in 96-well plates. To perform the MTT assay, cells were incubated with medium plus MTT (0.5mg/ml) at 37°C for 30-45min. Medium was removed and cells were lysed in DMSO. Sorensen solution (0.1M glycine, 0.1M NaCl, pH 10.5 in water) was added and absorbance measured at 570nm. For the clonogenic assay, cells were trypsinized after 72h of treatment and re-plated at equal numbers in 6-well plates. Colonies

were allowed to grow for two weeks in normal growth medium followed by fixation and staining of the colonies with 0.05% crystal violet in 30% ethanol. Colony numbers were measured with ColCount (Oxford Optronix).

Long-lived protein degradation assay

Cells were seeded in 24-well plates, radiolabeled with 0.1µCi ^{14}C-valine per mL (L-[U-14-C] valine; code CFB.75, Amersham) for 48h and treated with sunitinib for 24h. Remaining ^{14}C-valine was removed and cells were incubated for 1h in medium supplemented with 10mM L-valine. During this incubation time short-lived proteins were degraded. After washing, cells were incubated with medium supplemented with 10mM L-valine and with or without BafA1 for 5.5h, in which long-lived proteins were degraded. Supernatant and trypsinized cells were collected and acid precipitation and centrifugation were performed to separate supernatant and pellet. Fractions were mixed with Microscint40 and radioactivity was measured by liquid scintillation counting. Percentage of proteolysis of long-lived proteins was calculated from supernatant and pellet fractions.

Immunoblotting & Immunofluorescence

Cells were lysed in urea buffer (8M urea, 0.5% Triton X-100) supplemented with protease inhibitors (Roche). 40-60µg of protein was loaded on a 12% SDS-PAGE gel (Biorad) and then transferred to a PVDF membrane (Biorad). Incubation with primary antibodies was performed overnight at 4°C, followed by washing steps and incubation with secondary antibodies (DyLight 650 conjugate goat anti-rabbit and DyLight 550 conjugate goat anti-mouse, ImmunoReagents and Peroxidase-conjugated AffiniPure donkey anti-rabbit and donkey anti-mouse, Jackson ImmunoResearch) for 1h at room temperature. Chemiluminescent or fluorescent signal was detected using ChemiDoc MP System (Biorad). Total protein expression for quantification of specific protein expression was measured by use of the stain-free gel technology and imaged with the Chemidoc MP System (29).

Author Manuscript Published OnlineFirst on July 20, 2017; DOI: 10.1158/1535-7163.MCT-17-0136
Author manuscripts have been peer reviewed and accepted for publication but have not yet been edited.

For immunofluorescence, cells were plated on poly-L-lysine coated coverslips and treated for 24-48h. Fixation and immunofluorescence for galectin 3 was performed as described.(30) As secondary antibody goat anti-mouse Alexa Fluor 568 conjugate (Invitrogen) was used. Analysis was performed at a microscope Zeiss Axioplan 2 at x40 magnification. Samples were blinded and percentage of positive cells was calculated from 500-600 counted cells on randomly chosen fields in the DAPI channel.

Lysotracker staining

Cells were incubated in coated glass-bottom plates and treated with sunitinib for 72h. Medium was replaced by medium containing 100nM Lysotracker Red DND-99 (L7528, Molecular Probes) and cells were incubated for 1h at 37°C. Medium was exchanged to normal medium and cells were imaged at a confocal microscope Olympus FluoView-1000 at x63 magnification.

***In vivo* experiments**

Rip1Tag2 (C57BL/6) mice were kindly provided by G. Christofori, Basel, Switzerland. All experimental protocols were reviewed and approved by the Cantonal Veterinary Office of Bern (Switzerland). Mice were fed with food enriched in glucose starting from 10 weeks of age. Rip1Tag2 mice were treated daily from week 10 of age with 40mg/kg sunitinib p.o., 50mg/kg chloroquine i.p. or the respective vehicle control for three weeks. Animals were monitored daily. At 13 weeks of age, animals were euthanized, tumor number (>1mm) and size was measured, and tissues were fixed in formalin overnight and embedded in paraffin. Tumor volume was calculated using the formula $V=0.52*(width^2)*length$ to estimate the volume of a sphere (31). Tumor volume per mouse was calculated as the sum of single tumors.

Immunohistochemistry

For immunohistochemistry (IHC) and TUNEL (TdT-mediated dUTP nick end labeling) on mouse pancreas, tissues were cut in 4µm thick serial sections followed by deparaffinization,

rehydration and antigen retrieval using an automated immunostainer (Bond RX, Leica Biosystems). Antigen retrieval was performed for LC3B with Tris for 30 minutes at 95°C, for Ki67, SV40 and CD31 with citrate for 30 minutes at 95°C. Antibodies were diluted as follows: LC3B 1:4000, Ki67 1:400, SV40 1:100, CD31 1:100. For TUNEL, slides were incubated with TdT enzyme (Promega) for 20 minutes. Slides were counterstained with haematoxylin and eosin (H&E). For liver metastasis assessment, four step sections of 75µm were cut from liver tissue and stained with SV40 as described above. Number of metastasis was counted and summarized from all sections. Microvessel density (MVD) was evaluated by a staff pathologist (A.B.) based on IHC for CD31 and classified as high or low. Classification of tumors was performed based on H&E staining and according to classification criteria defined by Lopez and Hanahan (32). Necrosis was evaluated by a staff pathologist (A.B.) based on H&E staining, as percentage of area showing pre-necrotic condensed nuclei (regional cell death) and necrosis (geographic necrosis) compared to total tumor volume. Representative pictures of analyses for classification and necrosis on H&E staining are shown in supplementary figures S1A and S1B, respectively. Proliferation was measured as percentage of Ki67-positive cells compared to tumor volume in all tumors > 1mm and average per mouse is shown. Number of TUNEL-positive cells was counted in one high-power field chosen in the area of highest labeling. Autophagy was assessed by IHC for LC3B, classified according to the abundance and number of LC3B punctae, representative of autophagosomes (33). Mice were classified as either LC3B punctae low or LC3B punctae high. IHC for LC3B on 30 matched samples of human primary PanNET and liver metastasis (patient collective II as reported (34)) was performed as described above. Tumors were classified based on the abundance and number of LC3B punctae in absent, low or high LC3B punctae.

Statistical analysis

Statistical analyses were performed with GraphPad Software. Unpaired or paired t-test was used to compare groups. Contingency tables were analyzed using Fisher's exact test.

Sample size (n) refers to biological replicates unless otherwise stated. * p<0.05, ** p<0.01, *** p<0.001, **** p<0.0001.

Results

Sunitinib upregulates autophagy in PanNET cell lines and primary cells

We assessed sunitinib effects on autophagy in PanNET cell lines by immunoblotting for microtubule associated protein 1 light chain 3B (MAP1LC3B/LC3B). The cytosolic form LC3B-I is lipidated to LC3B-II, which is incorporated into autophagosomes and represents autophagosome numbers. Sunitinib treatment alone increased LC3B-II levels in both BON1 and QGP1 cells. To measure the autophagic flux we co-treated the cells with the lysosomal autophagy inhibitors chloroquine (CQ) or bafilomycin A1 (BafA1) (35), which block the fusion of autophagosomes with lysosomes via elevation of lysosomal pH. In both cell lines, LC3B-II levels further increased upon combination treatment of suntinib and autophagy inhibitors compared to single treatments alone, indicating increased autophagic flux. The effect was more prominent with CQ (Fig. 1A). Autophagy was also monitored by long-lived protein degradation assay (LLPDA) (20). Sunitinib increased autophagy-specific proteolysis in both cell lines (Fig. 1B, supplementary Fig. S2A). We assessed basal levels of autophagy in PanNET human tissue by immunohistochemistry for LC3B. LC3B punctae, representative for autophagosomes, significantly increased in liver metastasis compared to matched primary tumors, potentially indicating high levels of autophagy in stage IV patients (Supplementary Fig. S2B). Importantly, also in primary cells freshly isolated from PanNET patients, sunitinib increased LC3B-II levels, which were further elevated with autophagy inhibition (Fig. 1C). In conclusion, sunitinib upregulates autophagy in PanNET cell lines and primary cells as measured by LC3B-II and proteolysis of long-lived proteins.

Reduced viability and recovery upon combination with autophagy inhibition

We hypothesized that sunitinib-induced autophagy may provide a pro-survival mechanism limiting sunitinib anti-tumoral effect and that combination with autophagy inhibitors might

have a beneficial effect in reducing cell viability. To address this hypothesis, we combined increasing doses of sunitinib with fixed concentrations of CQ and BafA1, the latter two not affecting cell viability (Fig. 1D). Sunitinib decreased BON1 and QGP1 cell viability in a dose-dependent manner. The effect on viability was similar in both cell lines and seemed to be independent of target receptor expression levels (Supplementary Fig. S3A and S3B). CQ further reduced cell viability when combined with 10μM sunitinib (Fig. 1D, Supplementary Fig. S3A). Further experiments in the cell lines were performed with these concentrations of sunitinib and CQ. In primary cells from two PanNET patients, both sunitinib and CQ decreased viability in a dose-dependent manner. Also in primary PanNET cells their combination led to an increased effect (Fig. 1E). Calculation of the coefficient of drug interaction (CDI) as described previously (28) indicated an additive effect of sunitinib and CQ treatment in patient I (CDI=1.01) and a trend towards a synergistic effect in patient II (CDI=0.83). Cell cycle analysis by FACS revealed that sunitinib induced a G1 cell cycle arrest in PanNET cell lines, while the cell cycle was not affected by CQ (Supplementary Fig. S3C). To assess the long-term effect and recovery from treatments a colony formation assay was used. Sunitinib combined with autophagy inhibition led to a significant 50% reduction in colony numbers (Fig. 1F).

Reduced tumor burden *in vivo* upon combination treatment

We next assessed if autophagy inhibition increases the anti-tumoral effect of sunitinib *in vivo* in Rip1Tag2 mice, a transgenic mouse model of PanNET. We started treatment of mice at 10 weeks of age, when tumors have developed and can be detected macroscopically (Fig. 2A). Mice were treated for three weeks with either vehicle, CQ (50 mg/kg, daily i.p.), sunitinib (40 mg/kg, daily p.o.) or a combination thereof (Figure 2A). A dose of 50 mg/kg CQ corresponds to the human equivalent dose of 250 mg, which is the starting dose of Phase I trials of CQ and HCQ in cancer (36,37). Fifty mg/kg CQ led to an increase of LC3 in a melanoma xenograft model and to intratumoral concentrations of CQ, which blocked autophagy efficiently *in vitro* (38). Tumor number was significantly reduced after combination treatment

compared to single treatments (sunitinib p=0.0045, CQ p=0.0480). Tumor volume was reduced by 50% after combination treatment compared to single treatments (sunitinib p=0.0527, CQ p=0.0050) (Fig. 2A). Importantly, tumor number and volume significantly increase during sunitinib treatment compared to the start at 10 weeks of age, but not during the combination treatment (Fig. 2A). Microvessel density was clearly reduced upon sunitinib and combination treatment and unchanged upon CQ treatment (Supplementary Fig. S4A). Proliferation did not change upon CQ treatment but decreased significantly with sunitinib (p=0.0224) and the combination treatment (p=0.0017) compared to vehicle treatment (Fig. 2B and 2C). In addition to reduced proliferation, necrosis was elevated in tumors treated with sunitinib (p=0.0005) or sunitinib and CQ (p=0.0003) compared to vehicle-treated tumors (Fig. 2D). The number of TUNEL-positive cells increased significantly upon sunitinib (p=0.0222) and the combination (p=0.0163) treatment (Fig. 2E, supplementary Fig. S4B). Tumor classification revealed that invasiveness decreased upon sunitinib and combination treatment (Supplementary Fig. S4C), while incidence of metastasis and number of metastases per mouse did not change (Supplementary Fig. S4D). Punctate LC3B positivity by immunohistochemistry was classified into low and high. The distribution of LC3B punctae low versus LC3B punctae high increased towards LC3B punctae high in single and combination treatments compared to vehicle (Fig. 2F), indicating an upregulation of autophagy by sunitinib also *in vivo*. In summary, combination treatment of suntinib and CQ leads to an increased anti-tumor effect compared to single treatments in a pre-clinical setting.

Beneficial effect of combination treatment is partially due to autophagy inhibition

To prove a direct role of autophagy in limiting sunitinib anti-tumoral effect we knocked down key autophagy proteins, autophagy-related protein 5 (ATG5), autophagy-related protein 7 (ATG7) and lysosome-associated membrane protein 2 (LAMP2) by lentiviral delivery of shRNA. ATG5 and ATG7 are involved in vesicle formation and lipidation of LC3, while LAMP2 is a glycoprotein localized on the lysosome membrane, which is involved in the fusion between autophagosome and lysosome as well as in chaperone-mediated autophagy.

Upon knockdown, protein levels and starvation-induced autophagic flux were both reduced (Supplementary Fig. S5A-D). Proliferation and colony formation were slightly reduced in cells with shATG5, shATG7 or shLAMP2 compared to control-transduced cells (Fig. 3B and 4B). Cells with shATG5 and shATG7 had reduced viability upon sunitinib treatment compared to control-transduced cells (Fig. 3A). Additionally, recovery of sunitinib-treated shATG5 and shATG7 cells was significantly reduced compared to control-transduced cells to a similar extent as observed with the combination of sunitinib and CQ (Fig. 3B and 3C). While neither sunitinib nor the autophagy inhibitors CQ and BafA1 alone induced apoptosis in BON1 cells, their combination led to cleavage of caspase 3 and poly ADP ribose polymerase (PARP) (Fig. 3D, supplementary Fig. S6A and S6B). Sunitinib treatment did not induce apoptosis in BON1 ATG5 knockdown cells, whereas in QGP1 cells knocking down ATG5 already induced apoptosis, which was further increased by sunitinib treatment. In both cell lines, sunitinib treatment of ATG7 knockdown cells induced apoptosis, but at lower levels compared to pharmacological inhibition of autophagy (Fig. 3D and 3E). In summary, knockdown of early autophagy genes ATG5 and ATG7 only partially phenocopied the effect observed with pharmacological inhibitors.

Interestingly, knockdown of the late autophagy gene LAMP2 better recapitulated the effect of pharmacological inhibition. Sunitinib treatment reduced viability of shLAMP2 cells compared to control-transduced cells (Fig. 4A) as well as cell recovery similarly to the combination treatment of sunitinib and CQ (Fig. 4B and 4C). Sunitinib treatment of shLAMP2 BON1 and QGP1 cells induced apoptosis to a level comparable or even stronger than combination with autophagy inhibitors (Fig. 4D and 4E). The strong effect observed on apoptosis upon sunitinib and LAMP2 knockdown compared to ATG5 and ATG7 knockdown prompted us to investigate closer the involvement of lysosomes in sunitinib mediated autophagy induction.

Effect of combination treatment depends on lysosome stability and is mediated by lysosomal membrane permeabilization

LAMP2 has been shown to contribute to lysosomal stability (14). Knockdown of LAMP2 sensitized BON1 and QGP1 cell lines towards CQ (Fig. 5A-C) and the sensitivity towards CQ seemed to be dependent on LAMP2 levels. BON1 cells with lower levels of LAMP2 were more sensitive to CQ than QGP1 (Fig. 5A-C). Based on these results we hypothesized that lysosomal stability is an important factor in the response towards sunitinib and chloroquine treatment. Sunitinib and chloroquine are both lysosomotropic drugs, which due to their structure accumulate in lysosomes (11). We confirmed the lysosomotropic property of sunitinib by demonstrating that it co-localized with Lysotracker Red in BON1 and QGP1 cells (Fig. 5D). Lysosomotropic drugs can induce lysosomal membrane permeabilization (LMP) leading to release of lysosomal content in the cytoplasm, which in turn can activate apoptosis (39-42), and autophagy (17-19). Immunofluorescence for galectin 1 or 3 is considered the gold standard for detecting LMP (19). Upon permeabilization of lysosomes, galectins translocates from the cytoplasm and bind to the glycocalyx in lysosomes, which can be detected by immunofluorescence as a dot-like staining (Fig. 5E). CQ alone did not induce LMP, while sunitinib alone significantly induced LMP after 48h treatment, quantified as percentage of galectin 3 positive cells. Combination treatment of BON1 cells with sunitinib and CQ significantly increased LMP after 24h and 48h (Fig. 5F). Accordingly, sunitinib-treated shLAMP2 cells showed a significant increase of LMP and to the same degree as observed in control-transduced cells treated with sunitinib and CQ (Fig. 5G). Together, our data indicates that reduction of lysosomal stability, as in shLAMP2 cells or upon combination of the lysosomotropic drugs sunitinib and CQ, promotes LMP-induced damage, which then triggers apoptosis.

Discussion

Options for anti-cancer therapy are limited for patients with stage IV PanNETs. Since 2011, sunitinib has been approved for treatment of advanced PanNETs but it has a limited efficacy (4). Here we investigated if autophagy is involved in resistance to suntinib and therefore could be a potential therapeutic target. We evaluated our hypothesis on the only two

PanNET cell lines available, although these cell lines only partially represent PanNET biology (43,44). However, no better *in vitro* PanNET model is currently available. Due to this limitation, we studied our hypothesis additionally in primary cells from two PanNET patients and *in vivo* in a well-studied transgenic mouse model of PanNET. In PanNET cell lines and a transgenic PanNET mouse model we demonstrated that sunitinib combined with the autophagy inhibitor CQ has a significantly enhanced anti-tumor effect compared to single treatment alone. Additionally, the beneficial effect of the combination treatment was confirmed in human primary cell culture, suggesting that these findings might be relevant for PanNET patients.

First, we showed that sunitinib increases autophagy *in vitro* in PanNET cell lines, in cells isolated from human PanNET tumors and *in vivo* in the Rip1Tag2 transgenic PanNET mouse model. Sunitinib alone led to an upregulation of LC3B-II levels corresponding to an increased number of autophagosomes in PanNET cell lines and primary cells. LC3B-II levels further elevated when autophagy was blocked with lysosomal inhibitors indicating increased autophagic flux. *In vivo*, the number of mice with high LC3B punctate staining, representative for autophagosomes, increased upon sunitinib. Previous studies on other tumor types *in vivo* and in patient samples also reported modulation of autophagy upon sunitinib treatment (45,46). In tumors, autophagy might be influenced by additional factors, which may also result from sunitinib's anti-angiogenic activity, such as hypoxia (47), and inflammation or acidosis (48,49). These can be only partially mimicked *in vitro*. To our knowledge autophagy has not been assessed in human PanNET yet. We showed by immunohistochemistry for LC3B that autophagy is present in PanNETs with increased levels in liver metastasis compared to primary tumors, suggesting autophagy as a potential target in stage IV patients.

We observed reduced cell recovery and induction of apoptosis in cell lines treated with the combination of sunitinib and CQ. Similarly, Eng et al. have shown a synergistic effect of sunitinib and CQ in reducing cell proliferation in a lung adenocarcinoma cell line (50). Combination of sunitinib with CQ in the Rip1Tag2 model led to an increased anti-tumoral

effect compared to single treatments alone, as measured by reduced tumor burden, reduced proliferation and increased necrosis. Importantly, tumor burden increased during sunitinib treatment compared to the start of the treatment, but did not during combination treatment, indicating that the combination treatment strongly impairs tumor development. All the sunitinib-treated tumors were less vascularized, however, there was no difference in CD31 staining upon combination with CQ. This suggests that the increased anti-tumoral effect by the combination therapy is not explained by an effect on angiogenesis, but rather due to a direct effect on the cancer cells. Indeed, sunitinib has been shown to reduce tumor cell proliferation *in vitro* (23,24,50).

Sunitinib treatment reduced histological signs of tumor invasiveness but the incidence and number of liver metastasis remained unchanged. Reported data on sunitinib-induced invasiveness and metastasis in the Rip1Tag2 model are however inconsistent. Sunitinib has been shown to lead to increased invasiveness and incidence of metastasis (8,9), while a recent publication reports no change in invasiveness and number of metastasis per mouse upon sunitinib treatment (51). One important difference among these studies including ours is the age of the mice and the duration of the treatment, which might affect invasiveness and metastasis formation. A possible genetic drift of the Rip1Tag2 mice after breeding in different laboratories for a long time might be another reason for the different results (51,52). In summary, our findings show an anti-tumor effect of the combination treatment *in vivo*.

Sunitinib combined with ATG5 or ATG7 knockdown resulted in little or almost no apoptosis activation, while sunitinib combined with lysosome-targeting autophagy inhibitors such as CQ, BafA1 or LAMP2 knockdown, induced apoptosis. Our data suggest that lysosomes are centrally involved in the combination effect of sunitinib and CQ. This is in agreement with other studies showing that sunitinib as well as CQ and LAMP2 knockdown destabilize lysosomes (12,14,40). Destabilization of lysosomes can lead to lysosomal membrane permeabilization (LMP), which in turn can trigger cell death or autophagy (17-19). In BON1 cells, sunitinib alone induced LMP, which was further increased by addition of CQ or upon

knockdown of LAMP2. In QGP1 only the combination of sunitinib and a high concentration of CQ induced LMP, while single treatments did not (Supplementary Fig. S7A). This different susceptibility towards LMP seems to correlate with autophagic flux. Indeed, when autophagic flux upon sunitinib treatment is assessed by calculating the difference with and without CQ or BafA1, the two cell lines showed different results. In both cell lines autophagic flux upon sunitinib increased if LC3B-II levels were measured upon CQ treatment, while the flux was reduced when measured upon BafA1 treatment (Supplementary Fig. S7B). Interestingly, in QGP1 cells a higher concentration of CQ than the one used in BON1 increased flux, while a lower concentration of CQ also reduced the flux. (Supplementary Fig. S7C). These data suggest that BON1 cells are more susceptible than QGP1 towards LMP and show sunitinib-induced autophagy, while in QGP1 cells sunitinib rather blocked autophagy. Indeed, a recent study showed that sunitinib has a dual, concentration-dependent effect on autophagy in BON1 cells and that the threshold concentration differs between cell lines (53). This difference between BON1 and QGP1 cell lines might be due to the different levels of LAMP2 which influence lysosomal stability and lysosomal membrane permeabilitation (14). Indeed, our data showed that LAMP2 knockdown sensitized both cell lines toward sunitinib or CQ treatment. Similarly, LAMP1 or LAMP2 knockdown sensitized osteosarcoma cells towards siramesine, a lysosomotropic drug (14).

Our *in vitro* data suggest that sunitinib has a dual effect on autophagy by both blocking and inducing autophagy. We propose that the determining factor for the net effect of inhibition and induction is lysosome stability, with lysosome instability favoring cell death. Of note, in this context CQ and LAMP2 knockdown, which block autophagy, also contribute to autophagy induction via their destabilizing effect on lysosomes. The effect of BafA1 on LMP seems to be controversial in our results as well as in the literature and is probably context-dependent. In contrast to CQ, BafA1 does not accumulate in lysosomes but elevates the pH via inhibition of vacuolar ATPase (20), BafA1 treatment was shown to induce a release of cathepsin D from lysosomes followed by activation of caspase 3 (54). On the other hand, pre-treatment with BafA1 can limit LMP induced by another drug (40,42,55). Interestingly,

BafA1 could revert sunitinib resistance resulting from lysosomal sequestration in renal and colon cancer cell lines (11).

Based on our data, we propose that sunitinib accumulates in lysosomes and induces LMP. Autophagy is upregulated for clearance of damaged lysosomes, leading to recovery of the cells, therefore playing a pro-survival role. Combination of sunitinib with CQ or shLAMP2 leads to a higher destabilization of lysosomes and increased LMP, which is associated with apoptosis-dependent cell death (Fig. 6).

Lysosomes are an attractive therapeutic target because cancer cell lysosomes are less stable and more prone to permeabilization (13). Many drugs approved for other diseases target lysosomes. Due to this property they might be exploited also as anti-cancer therapeutics (15). CQ, approved for treatment of malaria, is already tested in several clinical trials in combination with various anticancer treatments. In phase I clinical trials hydroxychloroquine (HCQ) led to a significant anti-tumor effect in combination with other therapeutics (36,37). A clinical phase I trial is ongoing for the combination of sunitinib and HCQ in advanced solid tumors that did not respond to chemotherapy (NCT00813423). Our study strongly supports the rationale of this combination for treatment of PanNET patients and their inclusion in such clinical trials.

Acknowledgements:

We would like to thank PD Dr. Deborah Stroka for critical comments on the manuscript, Dr. Mario Noti for help and advice with animal experiments, and the Translational Research Unit for cutting the slides and immunohistochemistry. Tissues were provided by the Tissue Bank Bern.

References

1. Halfdanarson TR, Rubin J, Farnell MB, Grant CS, Petersen GM. Pancreatic endocrine neoplasms: epidemiology and prognosis of pancreatic endocrine tumors. *Endocr Relat Cancer* **2008**;15:409-27
2. Strosberg JR, Fine RL, Choi J, Nasir A, Coppola D, Chen DT*, et al.* First-line chemotherapy with capecitabine and temozolomide in patients with metastatic pancreatic endocrine carcinomas. *Cancer* **2011**;117:268-75

3. Yao JC, Shah MH, Ito T, Bohas CL, Wolin EM, Van Cutsem E*, et al.* Everolimus for advanced pancreatic neuroendocrine tumors. *N Engl J Med* **2011**;364:514-23
4. Raymond E, Dahan L, Raoul JL, Bang YJ, Borbath I, Lombard-Bohas C*, et al.* Sunitinib malate for the treatment of pancreatic neuroendocrine tumors. *N Engl J Med* **2011**;364:501-13
5. Pietras K, Hanahan D. A multitargeted, metronomic, and maximum-tolerated dose "chemo-switch" regimen is antiangiogenic, producing objective responses and survival benefit in a mouse model of cancer. *J Clin Oncol* **2005**;23:939-52
6. Fjallskog ML, Lejonklou MH, Oberg KE, Eriksson BK, Janson ET. Expression of molecular targets for tyrosine kinase receptor antagonists in malignant endocrine pancreatic tumors. *Clin Cancer Res* **2003**;9:1469-73
7. La Rosa S, Uccella S, Finzi G, Albarello L, Sessa F, Capella C. Localization of vascular endothelial growth factor and its receptors in digestive endocrine tumors: correlation with microvessel density and clinicopathologic features. *Hum Pathol* **2003**;34:18-27
8. Paez-Ribes M, Allen E, Hudock J, Takeda T, Okuyama H, Vinals F*, et al.* Antiangiogenic therapy elicits malignant progression of tumors to increased local invasion and distant metastasis. *Cancer Cell* **2009**;15:220-31
9. Sennino B, Ishiguro-Oonuma T, Wei Y, Naylor RM, Williamson CW, Bhagwandin V*, et al.* Suppression of tumor invasion and metastasis by concurrent inhibition of c-Met and VEGF signaling in pancreatic neuroendocrine tumors. *Cancer Discov* **2012**;2:270-87
10. Allen E, Mieville P, Warren CM, Saghafinia S, Li L, Peng MW*, et al.* Metabolic Symbiosis Enables Adaptive Resistance to Anti-angiogenic Therapy that Is Dependent on mTOR Signaling. *Cell Rep* **2016**;15:1144-60
11. Gotink KJ, Broxterman HJ, Labots M, de Haas RR, Dekker H, Honeywell RJ*, et al.* Lysosomal sequestration of sunitinib: a novel mechanism of drug resistance. *Clin Cancer Res* **2011**;17:7337-46
12. Ellegaard AM, Groth-Pedersen L, Oorschot V, Klumperman J, Kirkegaard T, Nylandsted J*, et al.* Sunitinib and SU11652 inhibit acid sphingomyelinase, destabilize lysosomes, and inhibit multidrug resistance. *Mol Cancer Ther* **2013**;12:2018-30
13. Fehrenbacher N, Gyrd-Hansen M, Poulsen B, Felbor U, Kallunki T, Boes M*, et al.* Sensitization to the lysosomal cell death pathway upon immortalization and transformation. *Cancer Res* **2004**;64:5301-10
14. Fehrenbacher N, Bastholm L, Kirkegaard-Sorensen T, Rafn B, Bottzauw T, Nielsen C*, et al.* Sensitization to the lysosomal cell death pathway by oncogene-induced down-regulation of lysosome-associated membrane proteins 1 and 2. *Cancer Res* **2008**;68:6623-33
15. Petersen NH, Olsen OD, Groth-Pedersen L, Ellegaard AM, Bilgin M, Redmer S*, et al.* Transformation-associated changes in sphingolipid metabolism sensitize cells to lysosomal cell death induced by inhibitors of acid sphingomyelinase. *Cancer Cell* **2013**;24:379-93
16. Hamalisto S, Jaattela M. Lysosomes in cancer-living on the edge (of the cell). *Curr Opin Cell Biol* **2016**;39:69-76
17. Hung YH, Chen LM, Yang JY, Yang WY. Spatiotemporally controlled induction of autophagy-mediated lysosome turnover. *Nat Commun* **2013**;4:2111
18. Maejima I, Takahashi A, Omori H, Kimura T, Takabatake Y, Saitoh T*, et al.* Autophagy sequesters damaged lysosomes to control lysosomal biogenesis and kidney injury. *EMBO J* **2013**;32:2336-47
19. Aits S, Kricker J, Liu B, Ellegaard AM, Hamalisto S, Tvingsholm S*, et al.* Sensitive detection of lysosomal membrane permeabilization by lysosomal galectin puncta assay. *Autophagy* **2015**;11:1408-24
20. Klionsky DJ, Abdelmohsen K, Abe A, Abedin MJ, Abeliovich H, Acevedo Arozena A*, et al.* Guidelines for the use and interpretation of assays for monitoring autophagy (3rd edition). *Autophagy* **2016**;12:1-222
21. Galluzzi L, Pietrocola F, Bravo-San Pedro JM, Amaravadi RK, Baehrecke EH, Cecconi F*, et al.* Autophagy in malignant transformation and cancer progression. *EMBO J* **2015**;34:856-80

22. Ikeda T, Ishii KA, Saito Y, Miura M, Otagiri A, Kawakami Y*, et al.* Inhibition of autophagy enhances sunitinib-induced cytotoxicity in rat pheochromocytoma PC12 cells. *J Pharmacol Sci* **2013**;121:67-73
23. Santoni M, Amantini C, Morelli MB, Liberati S, Farfariello V, Nabissi M*, et al.* Pazopanib and sunitinib trigger autophagic and non-autophagic death of bladder tumour cells. *Br J Cancer* **2013**;109:1040-50
24. Giuliano S, Cormerais Y, Dufies M, Grepin R, Colosetti P, Belaid A*, et al.* Resistance to sunitinib in renal clear cell carcinoma results from sequestration in lysosomes and inhibition of the autophagic flux. *Autophagy* **2015**;11:1891-904
25. Rovithi M, de Haas RR, Honeywell RJ, Poel D, Peters GJ, Griffioen AW*, et al.* Alternative scheduling of pulsatile, high dose sunitinib efficiently suppresses tumor growth. *J Exp Clin Cancer Res* **2016**;35:138
26. Amaravadi R, Kimmelman AC, White E. Recent insights into the function of autophagy in cancer. *Genes & Development* **2016**;30:1913-30
27. Tschan MP, Fischer KM, Fung VS, Pirnia F, Borner MM, Fey MF*, et al.* Alternative splicing of the human cyclin D-binding Myb-like protein (hDMP1) yields a truncated protein isoform that alters macrophage differentiation patterns. *J Biol Chem* **2003**;278:42750-60
28. Li X, Lin Z, Zhang B, Guo L, Liu S, Li H*, et al.* β-elemene sensitizes hepatocellular carcinoma cells to oxaliplatin by preventing oxaliplatin-induced degradation of copper transporter 1. *Scientific Reports* **2016**;6:21010
29. Taylor SC, Berkelman T, Yadav G, Hammond M. A defined methodology for reliable quantification of Western blot data. *Mol Biotechnol* **2013**;55:217-26
30. Aits S, Jaattela M, Nylandsted J. Methods for the quantification of lysosomal membrane permeabilization: a hallmark of lysosomal cell death. *Methods Cell Biol* **2015**;126:261-85
31. Inoue M, Hager JH, Ferrara N, Gerber HP, Hanahan D. VEGF-A has a critical, nonredundant role in angiogenic switching and pancreatic beta cell carcinogenesis. *Cancer Cell* **2002**;1:193-202
32. Lopez T, Hanahan D. Elevated levels of IGF-1 receptor convey invasive and metastatic capability in a mouse model of pancreatic islet tumorigenesis. *Cancer Cell* **2002**;1:339-53
33. Schlafli AM, Berezowska S, Adams O, Langer R, Tschan MP. Reliable LC3 and p62 autophagy marker detection in formalin fixed paraffin embedded human tissue by immunohistochemistry. *Eur J Histochem* **2015**;59:2481
34. Marinoni I, Kurrer AS, Vassella E, Dettmer M, Rudolph T, Banz V*, et al.* Loss of DAXX and ATRX are associated with chromosome instability and reduced survival of patients with pancreatic neuroendocrine tumors. *Gastroenterology* **2014**;146:453-60 e5
35. Gagliardi S, Gatti PA, Belfiore P, Zocchetti A, Clarke GD, Farina C. Synthesis and Structure−Activity Relationships of Bafilomycin A1 Derivatives as Inhibitors of Vacuolar H+-ATPase. *Journal of Medicinal Chemistry* **1998**;41:1883-93
36. Rangwala R, Chang YC, Hu J, Algazy KM, Evans TL, Fecher LA*, et al.* Combined MTOR and autophagy inhibition: phase I trial of hydroxychloroquine and temsirolimus in patients with advanced solid tumors and melanoma. *Autophagy* **2014**;10:1391-402
37. Vogl DT, Stadtmauer EA, Tan KS, Heitjan DF, Davis LE, Pontiggia L*, et al.* Combined autophagy and proteasome inhibition: a phase 1 trial of hydroxychloroquine and bortezomib in patients with relapsed/refractory myeloma. *Autophagy* **2014**;10:1380-90
38. Maes H, Kuchnio A, Peric A, Moens S, Nys K, De Bock K*, et al.* Tumor vessel normalization by chloroquine independent of autophagy. *Cancer Cell* **2014**;26:190-206
39. Kagedal K, Zhao M, Svensson I, Brunk UT. Sphingosine-induced apoptosis is dependent on lysosomal proteases. *Biochem J* **2001**;359:335-43
40. Boya P, Gonzalez-Polo RA, Poncet D, Andreau K, Vieira HL, Roumier T*, et al.* Mitochondrial membrane permeabilization is a critical step of lysosome-initiated apoptosis induced by hydroxychloroquine. *Oncogene* **2003**;22:3927-36
41. Cirman T, Oresic K, Mazovec GD, Turk V, Reed JC, Myers RM*, et al.* Selective disruption of lysosomes in HeLa cells triggers apoptosis mediated by cleavage of Bid by multiple papain-like lysosomal cathepsins. *J Biol Chem* **2004**;279:3578-87

42. Li Y, Chen M, Xu Y, Yu X, Xiong T, Du M*, et al.* Iron-Mediated Lysosomal Membrane Permeabilization in Ethanol-Induced Hepatic Oxidative Damage and Apoptosis: Protective Effects of Quercetin. *Oxid Med Cell Longev* **2016**;2016:4147610
43. Vandamme T, Peeters M, Dogan F, Pauwels P, Van Assche E, Beyens M*, et al.* Whole-exome characterization of pancreatic neuroendocrine tumor cell lines BON-1 and QGP-1. *Journal of Molecular Endocrinology* **2015**;54:137-47
44. Boora GK, Kanwar R, Kulkarni AA, Pleticha J, Ames M, Schroth G*, et al.* Exome-level comparison of primary well-differentiated neuroendocrine tumors and their cell lines. *Cancer Genet* **2015**;208:374-81
45. Abdel-Aziz AK, Mantawy EM, Said RS, Helwa R. The tyrosine kinase inhibitor, sunitinib malate, induces cognitive impairment in vivo via dysregulating VEGFR signaling, apoptotic and autophagic machineries. *Exp Neurol* **2016**;283:129-41
46. Spagnuolo RD, Brich S, Bozzi F, Conca E, Castelli C, Tazzari M*, et al.* Sunitinib-induced morpho-functional changes and drug effectiveness in malignant solitary fibrous tumours. *Oncotarget* **2016**
47. Bellot G, Garcia-Medina R, Gounon P, Chiche J, Roux D, Pouyssegur J*, et al.* Hypoxia-induced autophagy is mediated through hypoxia-inducible factor induction of BNIP3 and BNIP3L via their BH3 domains. *Mol Cell Biol* **2009**;29:2570-81
48. Zhong Z, Sanchez-Lopez E, Karin M. Autophagy, Inflammation, and Immunity: A Troika Governing Cancer and Its Treatment. *Cell* **2016**;166:288-98
49. Wojtkowiak JW, Gillies RJ. Autophagy on acid. *Autophagy* **2012**;8:1688-9
50. Eng CH, Wang Z, Tkach D, Toral-Barza L, Ugwonali S, Liu S*, et al.* Macroautophagy is dispensable for growth of KRAS mutant tumors and chloroquine efficacy. *Proc Natl Acad Sci U S A* **2016**;113:182-7
51. Bill R, Fagiani E, Zumsteg A, Antoniadis H, Johansson D, Haefliger S*, et al.* Nintedanib Is a Highly Effective Therapeutic for Neuroendocrine Carcinoma of the Pancreas (PNET) in the Rip1Tag2 Transgenic Mouse Model. *Clin Cancer Res* **2015**;21:4856-67
52. Singh M, Couto SS, Forrest WF, Lima A, Cheng JH, Molina R*, et al.* Anti-VEGF antibody therapy does not promote metastasis in genetically engineered mouse tumour models. *J Pathol* **2012**;227:417-30
53. Elgendy M, Abdel-Aziz AK, Renne SL, Bornaghi V, Procopio G, Colecchia M*, et al.* Dual modulation of MCL-1 and mTOR determines the response to sunitinib. *J Clin Invest* **2016**
54. Nakashima S, Hiraku Y, Tada-Oikawa S, Hishita T, Gabazza EC, Tamaki S*, et al.* Vacuolar H+-ATPase inhibitor induces apoptosis via lysosomal dysfunction in the human gastric cancer cell line MKN-1. *J Biochem* **2003**;134:359-64
55. Seitz C, Hugle M, Cristofanon S, Tchoghandjian A, Fulda S. The dual PI3K/mTOR inhibitor NVP-BEZ235 and chloroquine synergize to trigger apoptosis via mitochondrial-lysosomal cross-talk. *Int J Cancer* **2013**;132:2682-93

Figure legends

Figure 1: **Sunitinib modulates autophagy in PanNET cell lines and primary cells and combination with autophagy inhibition reduces viability and recovery**

A. Representative immunoblot for LC3B in BON1 and QGP1 cells upon 24h sunitinib (10μM), 24h CQ (20μM in BON1, 50μM in QGP1), 5.5h BafA1 (200nM). LC3B-II levels were normalized to GAPDH or total protein, n≥4. **B**. Autophagic flux in BON1 and QGP1 cells calculated from percentage of proteolysis in long-lived protein degradation assay (treatment with BafA1 – treatment without BafA1), n=4. **C**. Immunoblots for LC3B in primary cells isolated from PanNET patients I and II upon 7h sunitinib (10μM), 7h CQ (20μM), 2h BafA1 (200nM). LC3B-II levels were normalized to total protein and are indicated below the corresponding LC3B-II immunoblot, n=1. **D**. Viability of BON1 and QGP1 cells upon treatment. MTT assay was performed after 72h treatment with sunitinib (10μM), CQ (BON1 20μM, QGP1 50μM), BafA1 (20nM) and values were normalized to control, n≥2. **E**. Viability of primary cells isolated from PanNET patients I and II upon treatment. ATPlite assay was performed after 48h treatments with indicated concentrations of CQ and sunitinib and values were normalized to control, n=1, error bars show technical replicates. **F**. Representative picture and quantification of clonogenic assay in BON1 cells. The image shows triplicates for each treatment of one representative experiment. Colonies were fixed and stained after two weeks without treatment and colony numbers were normalized to control, n≥3. Statistical analysis was performed using unpaired t-test, * $p<0.05$, ** $p<0.01$, *** $p<0.001$, **** $p<0.0001$.

Figure 2: Significant anti-tumor effect *in vivo* upon combination treatment

A. Graphic representation of the mouse treatment and macroscopically assessed tumor volume and number in Rip1Tag2 mice at 10 weeks of age and after three weeks of daily treatment with vehicle, CQ, sunitinib or sunitinib + CQ (10 weeks n=10, vehicle n=13, CQ n=12, sunitinib n=12, sunitinib + CQ n=12), unpaired t-test. **B**. Immunohistochemical staining for the proliferation marker Ki67. Percentage of Ki67 positive cells was estimated in 3-14 tumors >1mm per mouse as shown in representative pictures with corresponding percentage

of positive cells. **C**. Quantification of Ki67 staining. The graph shows the mean percentage of positive cells per mouse (vehicle n=13, CQ n=12, sunitinib n=12, sunitinib + CQ n=12), unpaired t-test. **D**. Quantification of percentage of necrosis determined on H&E staining (vehicle n=13, CQ n=12, sunitinib n=12, sunitinib + CQ n=12), unpaired t-test. **E**. Quantification of number of TUNEL-positive cells/mm^2 as determined in one high-power field per mouse (vehicle n=13, CQ n=12, sunitinib n=12, sunitinib + CQ n=12). **F**. Immunohistochemical staining for LC3B. Classification of each mouse in LC3B punctae high or low based on abundance of dot staining as shown in representative pictures (LC3B punctae low: no dots in most of the tumors, LC3B punctae high: dots in most of the tumors). The graph presents the percentage of mice with LC3B high/low punctate staining (vehicle n=13, CQ n=12, sunitinib n=12, sunitinib + CQ n=12), Fisher's exact test. * p<0.05, ** p<0.01, *** p<0.001, **** p<0.0001.

Figure 3: **Sunitinib treatment of shATG5 and shATG7 cells only partially phenocopies combination with chloroquine**

A. Viability of BON1 shControl, shATG5 and shATG7 cells upon treatment. MTT assay was performed after 72h treatment with sunitinib (10μM), CQ (20μM) and values were normalized to the respective DMSO control, n≥3. **B**. Representative pictures of clonogenic assay in BON1 shControl, shATG5 and shATG7 cells. Colonies were fixed and stained after two weeks without treatment. Triplicates of one representative experiment are shown for each treatment. **C**. Clonogenic assay in BON1 shControl, shATG5 and shATG7 cells. Colony numbers were normalized to the respective DMSO control, n≥3 **D**. Representative immunoblot for ATG5, ATG7, cleaved caspase 3 and cleaved PARP in BON1 shControl, shATG5 and shATG7 cells after 24h treatment with sunitinib (10μM), CQ (20μM), BafA1 (20nM), n=3. **E**. Representative immunoblot for ATG5, ATG7, cleaved caspase 3 and cleaved PARP in QGP1 shControl, shATG5 and shATG7 cells after 24h treatment with sunitinib (10μM), CQ (50μM), BafA1 (50nM), n=3.Statistical analysis was performed using unpaired t-test, * p<0.05, ** p<0.01, *** p<0.001, **** p<0.0001.

Figure 4: **Sunitinib treatment of shLAMP2 cells phenocopies combination with chloroquine**

A. Viability of BON1 shControl, shLAMP2-291 and shLAMP2-561 cells upon treatment. MTT assay was performed after 72h treatment with sunitinib (10µM), CQ (20µM) and values were normalized to the respective DMSO control, n≥3. **B**. Representative pictures of clonogenic assay in BON1 shControl, shLAMP2-291 and shLAMP2-561 cells. Colonies were fixed and stained after two weeks without treatment. Triplicates of one representative experiment are shown for each treatment. **C**. Clonogenic assay in BON1 shControl, shLAMP2-291 and shLAMP2-561 cells. Colony numbers were normalized to the respective DMSO control, n≥3 **D**. Representative immunoblot for LAMP2, cleaved caspase 3 and cleaved PARP in BON1 shControl, shLAMP2-291 and shLAMP2-561 after 24h treatment with sunitinib (10µM), CQ (20µM), BafA1 (20nM), n=3. **E**. Representative immunoblot for LAMP2, cleaved caspase 3 and cleaved PARP in QGP1 shControl, shLAMP2-291 and shLAMP2-561 after 24h treatment with sunitinib (10µM), CQ (50µM), n=3. Statistical analysis was performed using unpaired t-test, * $p<0.05$, ** $p<0.01$, *** $p<0.001$, **** $p<0.0001$.

Figure 5: **Effect of combination treatment depends on lysosome stability and is mediated by lysosomal membrane permeabilization**

A. Representative immunoblots for LAMP2 in BON1 and QGP1 shControl, shLAMP2-291 and shLAMP2-561 cells, n>3. **B**. Viability of BON1 shControl, shLAMP2-291 and shLAMP2-561 cells upon treatment. MTT assay was performed after 72h treatment with increasing concentrations of CQ (20µM, 50µM, 100µM) and values were normalized to the respective vehicle control, n=3. **C**. Viability of QGP1 shControl, shLAMP2-291 and shLAMP2-561 cells upon treatment. MTT assay was performed after 72h treatment with increasing concentrations of CQ (20µM, 50µM, 100µM) and values were normalized to the respective vehicle control, n=3. **D.** Representative images showing the co-localization of the sunitinib-autofluorescence (72h, 10µM) in the FITC channel and Lysotracker Red staining lysosomes (1h, 100nM) in the Cy3 channel. Scale bar 10µm, applies to all images. **E**. Representative immunofluorescent picture of a LMP-positive BON1 cell showing galectin 3 dotted staining

and a negative cell without dotted galectin 3 staining upon 48h sunitinib + CQ treatment. Nuclei were stained with DAPI. Scale bar 20µm. **F**. LMP in BON1 cells upon treatment. Percentage of galectin 3 positive cells upon 24h and 48h treatment with sunitinib (10µM) and CQ (20µM) was calculated from 500-600 counted cells in randomly chosen fields, n=5. **G**. LMP in BON1 shControl, shLAMP2-291 and shLAMP2-561 cells upon treatment. Percentage of galectin 3 positive cells upon 24h and 48h treatment with sunitinib (10µM) and CQ (20µM) was calculated from 500-600 counted cells in randomly chosen fields, n≥5. Statistical analysis was performed using unpaired t-test, * $p<0.05$, ** $p<0.01$, *** $p<0.001$, **** $p<0.0001$.

Figure 6: **Proposed model of sunitinib and combination effect**

Sunitinib accumulates in lysosomes and induces autophagy. Autophagy enables recovery of the cells, therefore playing a pro-survival role. If autophagy is blocked via knockdown of ATG5 or ATG7 in combination with sunitinib, reduced recovery is observed. Upon combination of sunitinib with CQ or LAMP2 knockdown, both combinations collaborate to a higher destabilization of lysosomes in addition to reduced recovery, leading to apoptosis-dependent cell death.

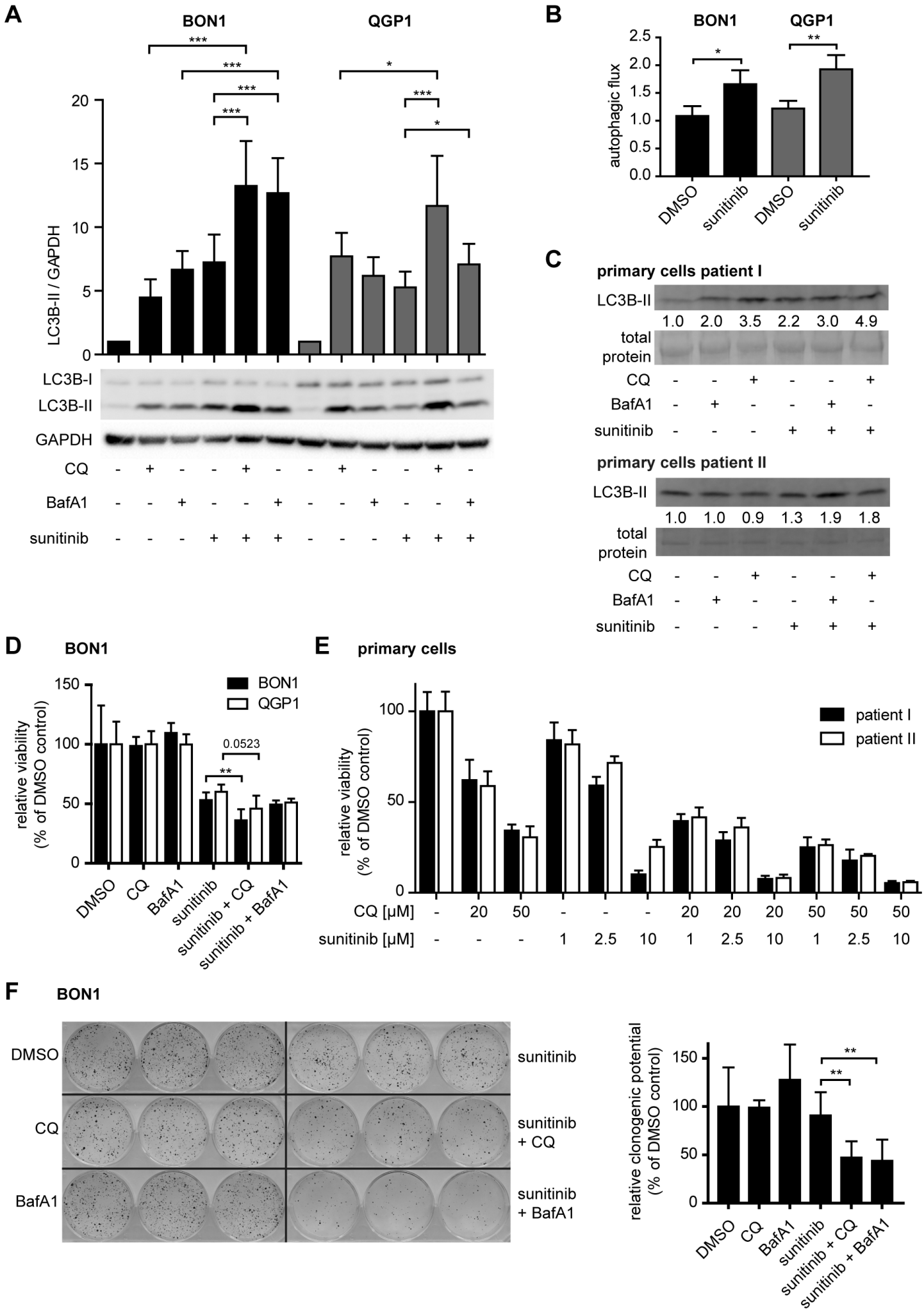

Figure 1

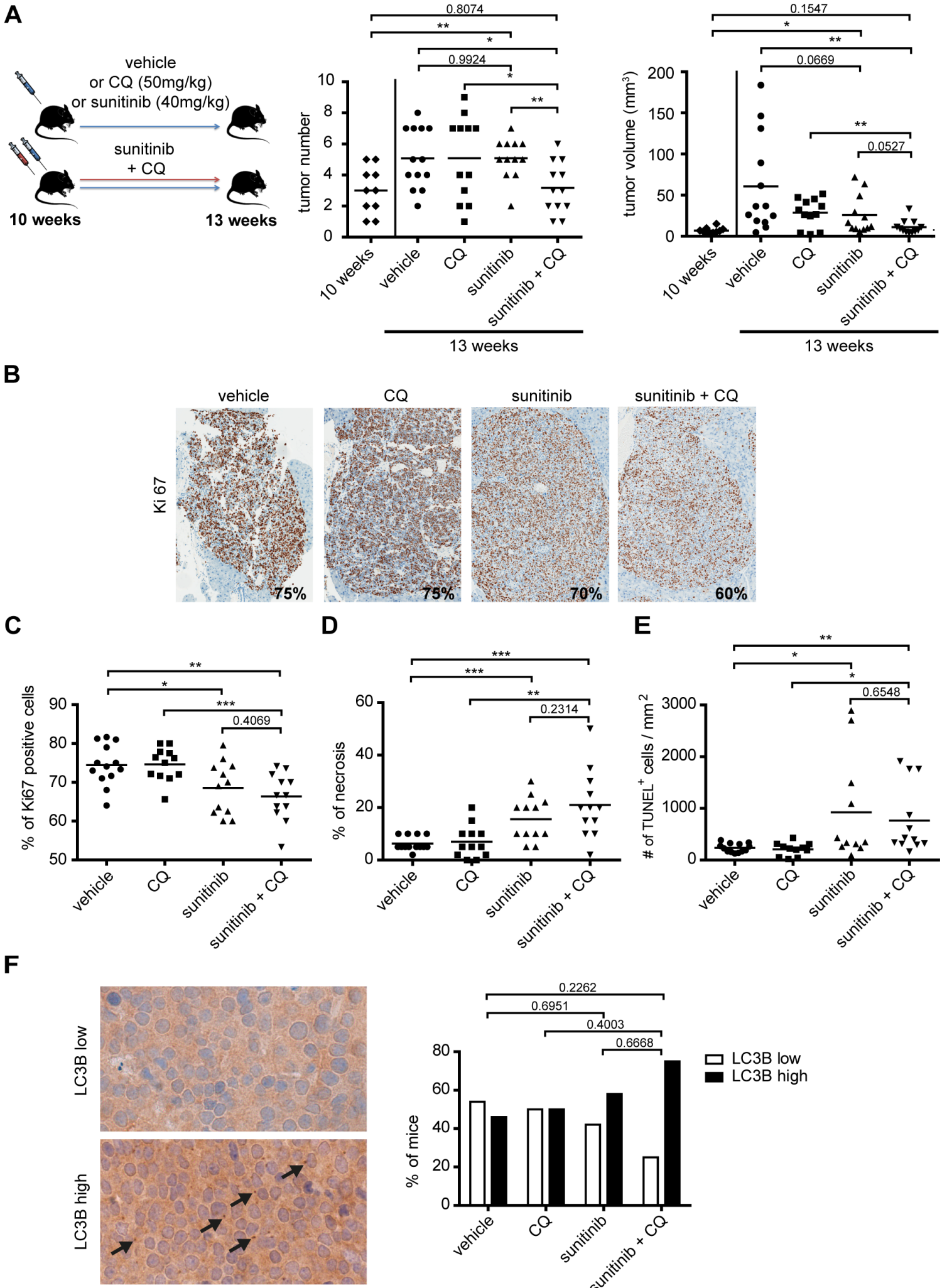

Figure 2

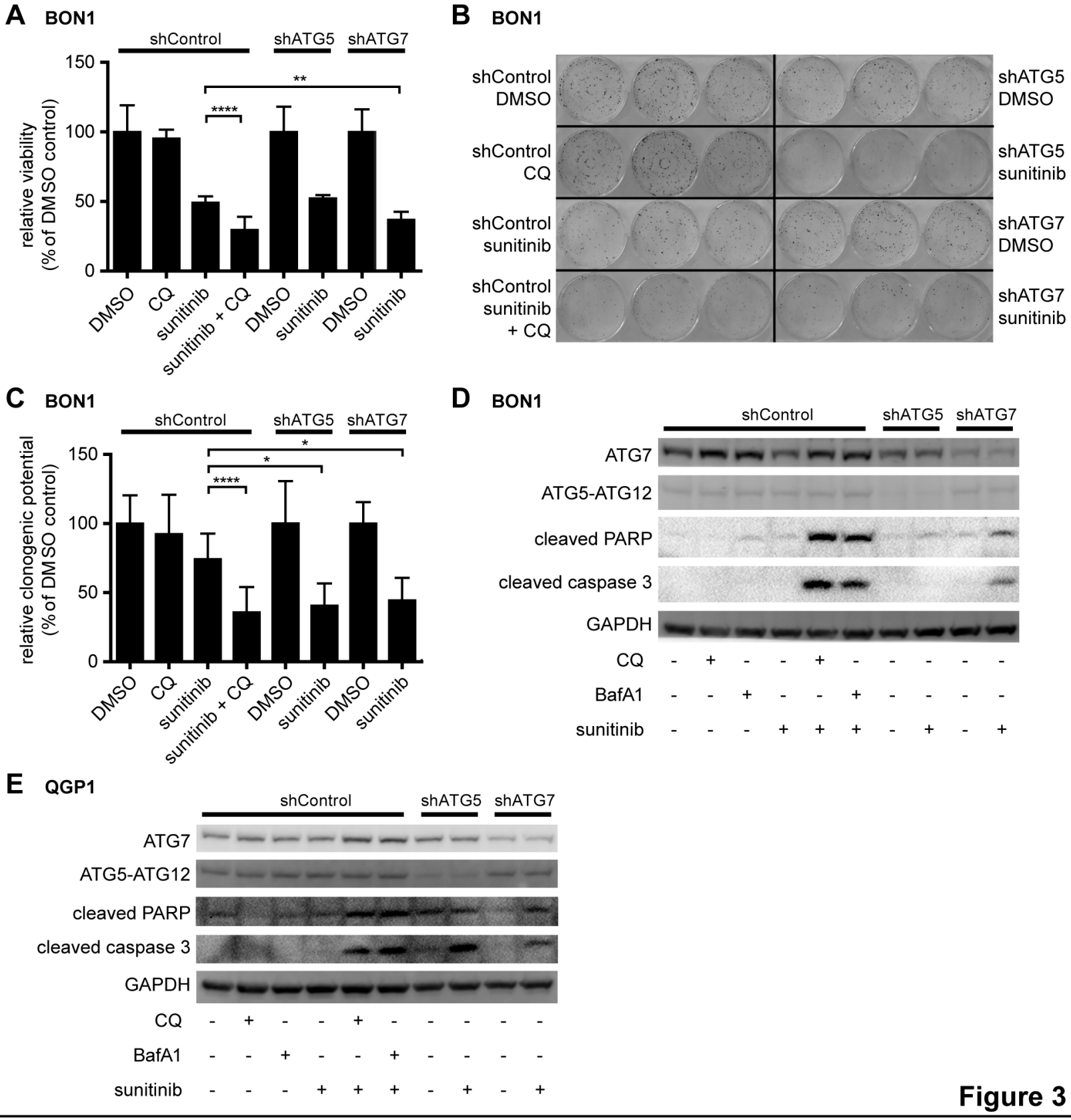

Figure 3

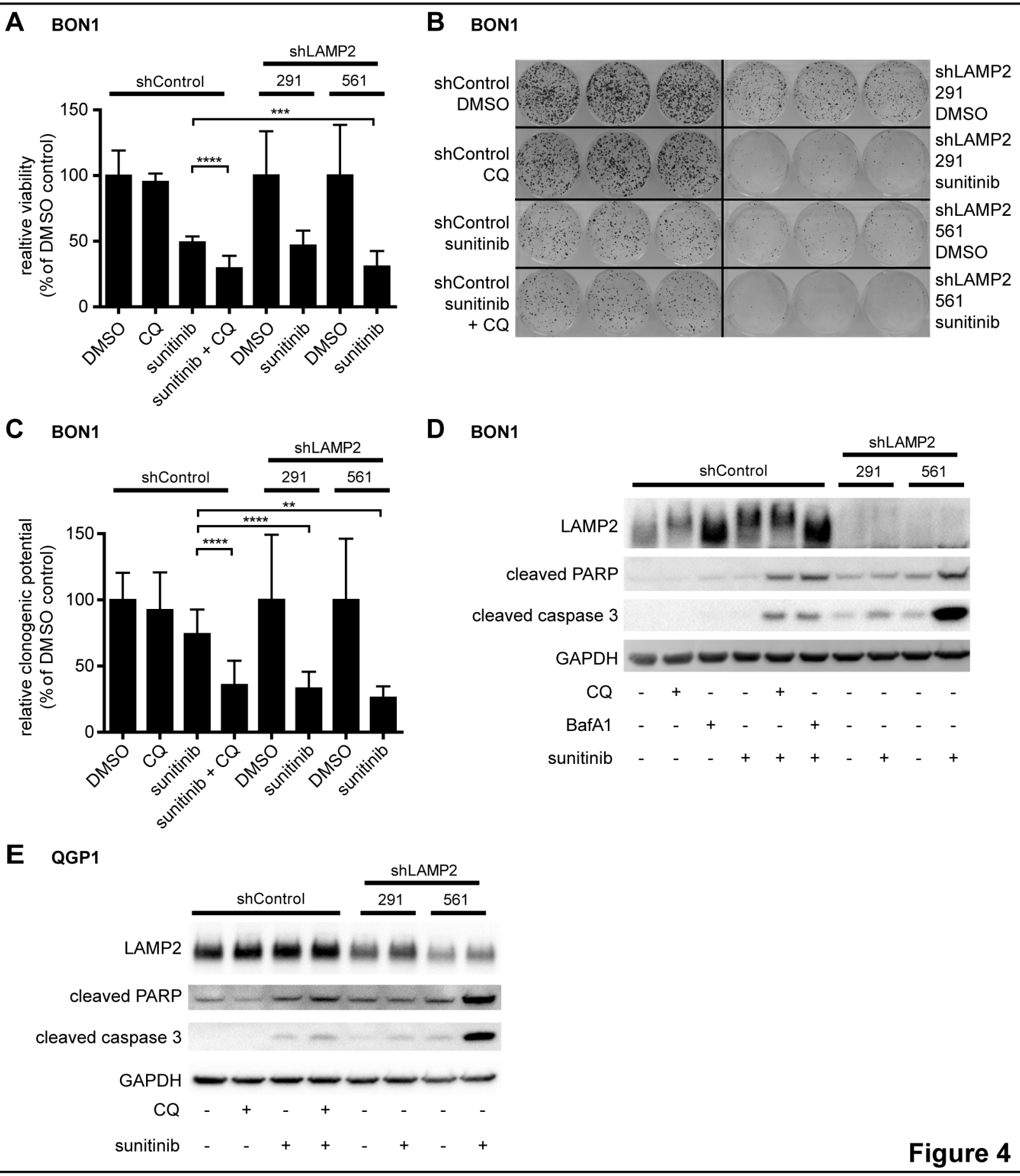

Figure 4

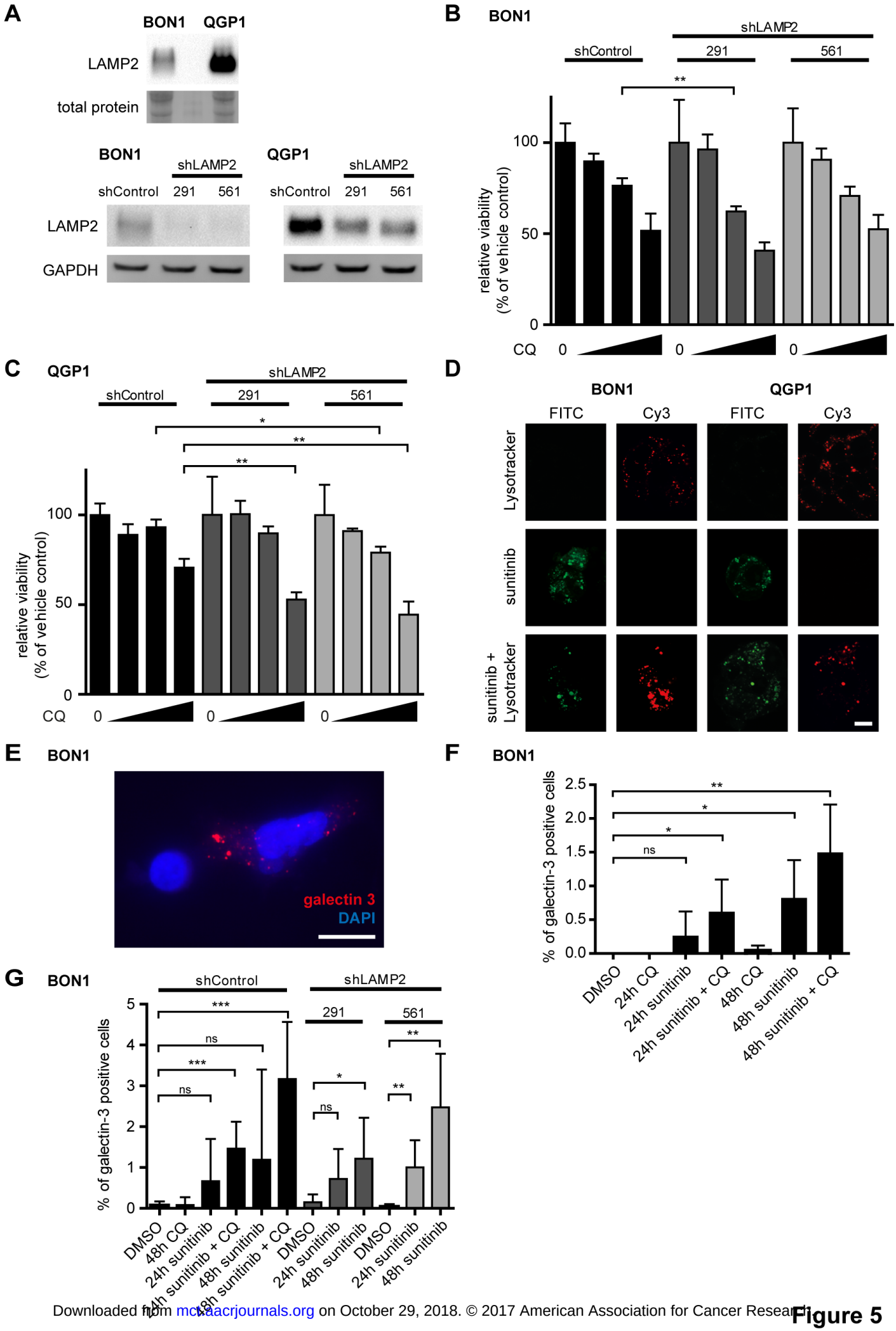

Figure 5

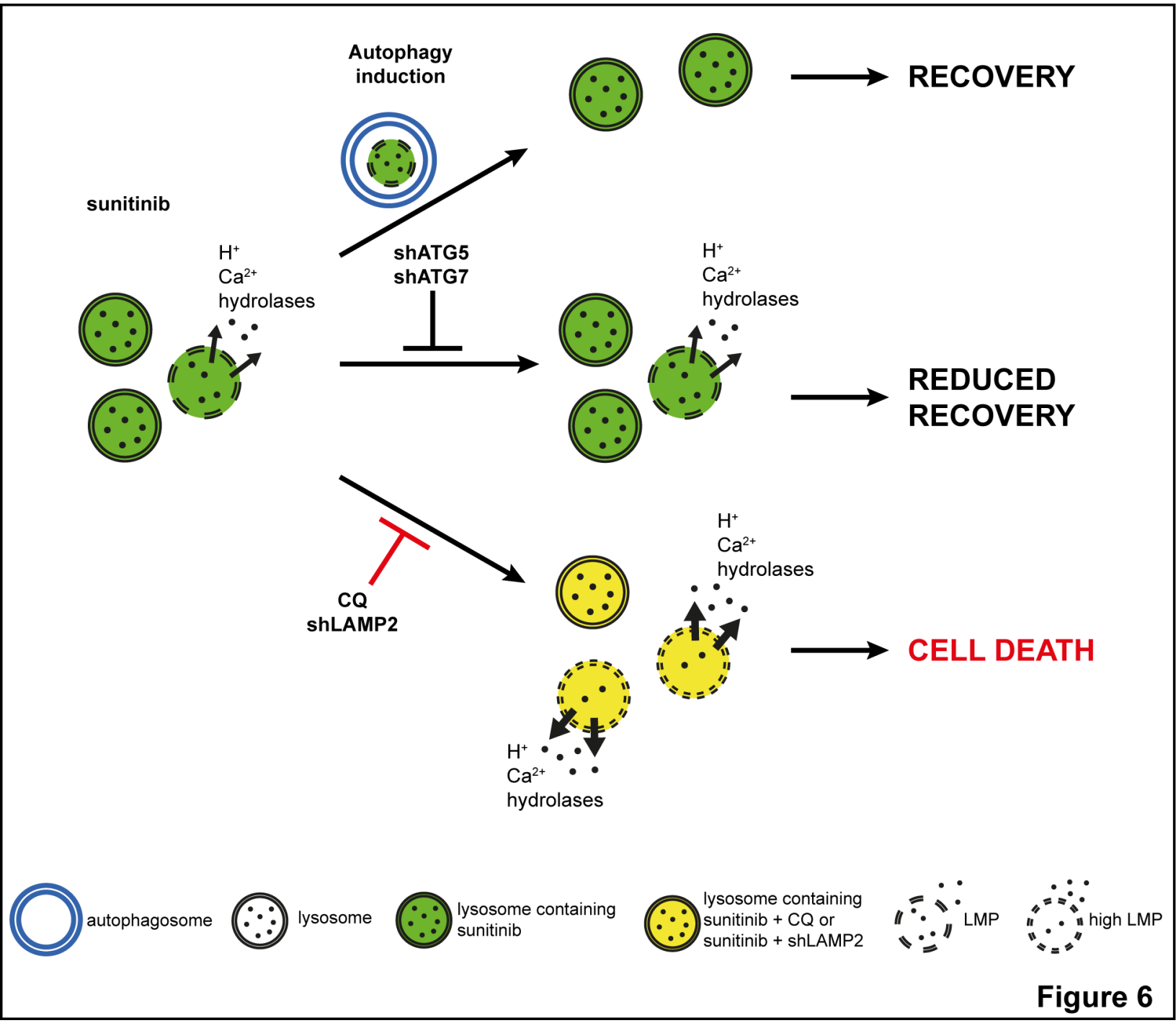

Figure 6

AACR American Association for Cancer Research

Molecular Cancer Therapeutics

Autophagy inhibition improves sunitinib efficacy in pancreatic neuroendocrine tumors via a lysosome-dependent mechanism

Tabea Wiedmer, Annika Blank, Sophia Pantasis, et al.

Mol Cancer Ther Published OnlineFirst July 20, 2017.